https://doi.org/10.5194/wes-2020-22
Preprint. Discussion started: 19 February 2020

eawe european academy of wind energy
Open Access WIND ENERGY SCIENCE DISCUSSIONS

Aero-elastic analysis of wind turbines under turbulent inflow conditions

Giorgia Guma[1], Galih Bangga[1], Thorsten Lutz[1], and Edwald Krämer[1]
[1]Institute of Aerodynamics and Gas Dynamics, University of Stuttgart, Pfaffenwaldring 21, 70569 Stuttgart, Germany
Correspondence: Giorgia Guma (guma@iag.uni-stuttgart.de)

Abstract. The aero-elastic response of the DANAERO wind turbine and interaction phenomena are investigated by the use of a high-fidelity model. A time-accurate unsteady fluid-structure interaction (FSI) coupling between a computational fluid dynamics (CFD) code for the aerodynamic response and a multi-body simulation (MBS) code for the structural response is used. Different CFD models of the same turbine with increasing complexity and technical details are coupled to the same MBS model in order to identify the impact of the different modeling approaches. The influence of the blade and tower flexibility and of the inflow turbulence is analyzed for a specific case of the DANAERO experiment. Lastly a fatigue analysis is performed from load signals in order to identify the most damaging load cycles and the fatigue ratio between the different models, showing that for low inflow velocities, a high turbulence has a major impact than the flexibility.

1 Introduction

The current design trend of wind turbines is leading to rotor diameters getting larger and larger, and therefore lighter in order to decrease the cost of wind power generations in terms of leveling energy costs ($\$/kWh$) and make it a competitive resource in comparison to other electric generations systems. Much research is done to investigate materials and construction techniques in order to allow lighter designs with the consequence that the rotor blades are becoming more and more flexible. In these cases, large deformations are occurring with consequent non-stationary loads and oscillations, resulting in unexpected changes in performances or even flutter if the damping is negative. Additionally, large rotor wind turbines are in reality subjected to diverse inflow conditions, such as shear, turbulence and complex terrain, leading to higher wind instabilities and fluctuations. Moreover, the aerolastic instabilities strongly affect the operational life of wind turbines (Hansen et al. (2006)). Most of the available simulation tools for wind turbines aeroelasticity are based on engineering models like BEM for the aerodynamics and 1D MBS for the structural response, like for example in Riziotis et al. (2008) and Jeong et al. (2011). These models are cheap but rely on different correction models to take unsteadiness and 3D effects into account, (Madsen et al. (2012)). In the recent years, high-fidelity FSI has been frequently used for wind turbine applications. Sayed et al. (2016) implemented a coupling of the CFD solver FLOWer to the CSD (Computational Structure Dynamics) solver Carat++, where the only blades have been coupled either to a 1D beam or a 2D shell structural model. Yu et al. (2014) used a loosed coupling CFD-CSD with an incompressible CFD solver and non-linear Euler-Bernoulli beam elements for the structure in order to investigate the aeroelastic response of the generic NREL 5 MW rotor. The communication in this case was only once per revolution. The

https://doi.org/10.5194/wes-2020-22
Preprint. Discussion started: 19 February 2020

same turbine was used also by Bazilevs et al. (2011b) and Hsu et al. (2012) by means of FSI between a low-order Arbitrary Lagrangian-Eulerian Variational Multi Scale (ALE-VMS) flow solver and a Non-Uniform Rational Basis Spline (NURBS) based structural solver. Again for the same turbine Heinz et al. (2016) coupled the flow solver Ellypsys3D to the aeroelastic solver HAWC2 and the compared to BEM results of HAWC2 alone. While he considered uniform inflow, Li et al. (2017) considered additionally a turbulent inflow synthetically generated by the use of a Mann box Mann (1994). Dose et al. (2018) presented a method to couple flow solver OpenFOAM to the FEM-based beam solver BeamFOAM. A CFD-MBS coupling between the URANS solver TURNS and the MBS solver MBDyn was used by Masarati et al. (2011) to investigate the NREL Phase VI rotor.

Wind turbines are especially susceptible to fatigue damage, because of the oscillating characteristic of the affecting loads. Fatigue analysis are normally performed by the manufacturers for certification purposes, and therefore they are mostly BEM-based. In the EU-project AVATAR (Schepers (2016)) it was shown that BEM-based calculations against high fidelity led to a 15% error in the computation of the fatigue. This error motivated the TKI WoZ VortexLoads project (Boorsma et al. (2019)), where starting from turbulent inflow conditions BEM based and CFD based calculation have been compared within each other and to experimental results.

In section 2 the high-fidelity framework (as presented in Klein et al. (2018)) is described for fluid-structure interaction coupled simulations on the NM80 2MW wind turbine rotor, also known as DANAERO rotor, (DANAERO). Additionally the inflow conditions and setup for the different cases are listed. Different setups are used with increasing complexity in order to recognize distinctively their effects. In section 3 the aeroelastic response of the reference turbine is shown and the variations between the models with different complexity is exposed. Lastly the Damage Equivalent Loading (DEL) calculation is performed in post processing of the different simulations, taking into account two different time varying input variables.

2 Methodology

2.1 DANAERO wind turbine

The DANAERO wind turbine rotor is taken into consideration for the following calculations. This is the reference wind turbine in the IEA Task 29 IV, also known as MEXNEXT IV, (IEA Task 29). In this project different institutions and universities around the world compare their own codes and approaches, applying them for the calculations planned into different subtasks of the same project. The results will not only be compared to each other, but also to the experimental results provided by the well known DANAERO experiment (Madsen et al. (2010)). These were conducted between 2007-2010 in cooperation between the Technical University of Denmark and the industrial partners Vestas, Siemesn LM and DONG Energy, and then post processed and calibrated in the follow up project DANAEROII, (Troldborg et al. (2013)). In this way it is possible not only to understand limitations and problematics of the different approaches, but also improve them. The turbine has a rotor diameter of around 80 m, a tilt angle of 5 degrees and around 1.4 m prebend. Hub, nacelle and tower have been reproduced as cylinders within the present study, based on the available diameter distribution provided in the structural model.

https://doi.org/10.5194/wes-2020-22
Preprint. Discussion started: 19 February 2020

eawe european academy of wind energy
Open Access WIND ENERGY SCIENCE DISCUSSIONS

2.2 CFD model and inflow conditions

The simulations are performed with the CFD code FLOWer (Raddatz (2009)). Firstly developed at the German Aerospace Center (DLR), FLOWer is now since many years expanded at the Institute of Aerodynamic and Gas Dynamic (IAG) for helicopter and wind turbine applications. It is a URANS and DES finite volume solver for structured meshes. The present simulations are run using the Shear-Stress-Transport (SST) k-omega according to Menter (Menter (1994)), considering a fully turbulent boundary layer. Two different spatial discretization schemes are available, a second order central cell-centered Jameson-Schmidt-Turkel (JST) ((Jameson et al.(1981)) and fifth order weighted essentially non-oscillatory (WENO) (Kowarsch et al. (2013)) scheme. The second one is applied in the present study on the background mesh in order to reduce the dissipation of the vortices. The time-stepping scheme is an artificial 5-stage Runge-Kutta scheme and multi-grid level 3 is applied to accelerate the convergence of the solution. The time integration scheme is the implicit procedure called dual-time stepping where at the beginning of each timestep t an estimation of the solution is guessed, and the closer it is to the real one, the smaller the necessary number of inner iterations to reach convergence. Independent grids need to be created for each single component, together combined by the use of the Chimera technique.

The CFD model of the blade is created from provided the CAD file, where a "water tight" outer surface is extracted. For the hub, nacelle and tower, surface databases are recreated (cylinder-based) from the provided geometrical properties. Meshes are generated by the use of the commercial software Pointwise in combination with in-house scripts. All components have been meshed ensuring $y^+ \approx 1$ in the boundary layer region. The blades are meshed in an O-mesh topology, with 257 points over the the profile and 201 points in radial direction, for a total of around 9 Mio cells for each blade. The background mesh consists of hanging grid nodes in which the component meshes are embedded by the use of the Chimera technique. Three different CFD models have been created for the turbine, with increasing fidelity:

1. One-third model (BMU) of the rotor (only one blade);
2. Full model of the turbine (FMU) including nacelle and tower suited for uniform inflow conditions;
3. Full model of the turbine (FMT) including nacelle and tower suited for turbulent inflow conditions;

The differences between the three lay on the used backgrounds of the models. Setup 1 has no ground, because it is just a 120° model of the turbine. Setup 2 has no friction on the ground in order to avoid the generation of a wind profile. Finally, setup 3 has friction on the ground in order to consequently propagate the sheared turbulent inflow and is much more expensive in comparison to case 2 (87 Mio cells against 58 Mio), because an additional refinement is added upwind where the turbulence is injected, and different boundary conditions need to be applied in order to ensure a correct propagation of the turbulence. The 120° model is much cheaper than the other two, because it uses the periodic characteristic of a 3-bladed wind turbine, but of course it considers no tilt angle nor tower influence. The different boundary conditions and CFD models are depicted in fig. 1, while in the following the meaning of the different boundary conditions is clarified:

- NAVIER-STOKES and EULER wall represent the ground with and without friction, respectively;

https://doi.org/10.5194/wes-2020-22
Preprint. Discussion started: 19 February 2020

eawe european academy of wind energy
Open Access WIND ENERGY SCIENCE DISCUSSIONS

- FARFIELD represents the uniform inflow boundary condition;
- PERIODIC/PERIODIC ROT represent the symmetrical boundary condition for the plane and 120° model, respectively;
- GUST is the Dirichlet boundary condition, by which arbitrary unsteady inflow can be applied;
- PRESSURE OUTLET defines the outflow based on the pressure;

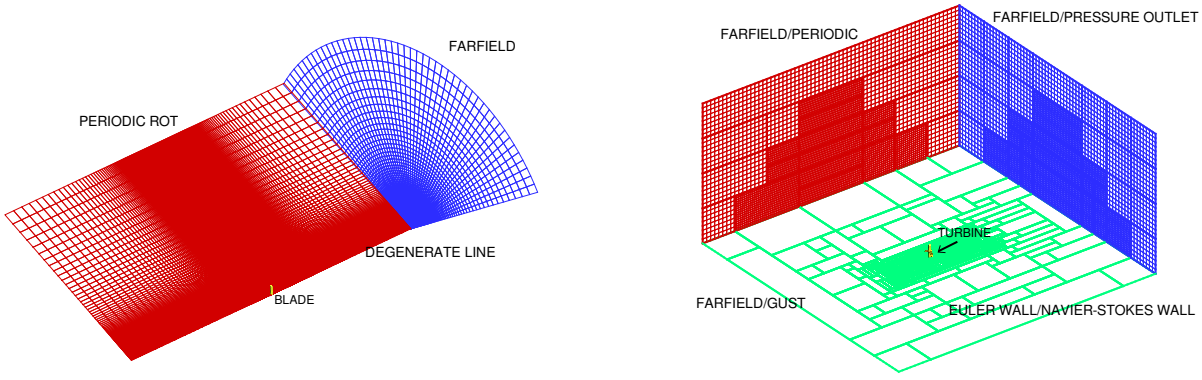

(a) BMU

(b) FMU/FMT

Figure 1. Details of the meshes and boundary conditions for BMU and FMU/FMT

All the simulations are run based on the conditions defined in the subtask 3.1 of the IEA task 29, see (IEA Task 29). This means with a rated inflow velocity of $6.1m/s$ in the uniform case. For FMT, synthetic turbulence is generated by the use of a Mann Box (Mann (1994)), where a Turbulence Intensity (TI) of 20% and a length scale of 0.59*hub height (as according to the IEC normative 61400) are preset. This is add to the flow in terms of body forces 4D upstream from the tower bottom, and therefore a mesh refinement of the background is applied from this point in order to allow a better propagation of the turbulence. Sheared inflow is superimposed by the use of a power law with $\alpha = 0.025$. Due to the low reference velocity considered during the DANAERO experiment, a really high TI was chosen in order to be able to identify distinctively the effects of a turbulent atmospheric boundary layer. DDES is used instead of URANS for the CFD solution, with accordingly changed in the boundary conditions.

2.3 MBS solver

2.3.1 Structural model

The multi-body dynamics (MBD) simulation code SIMPACK is used to simulate the structural dynamics of the turbine (as in Jassmann et al. (2014) and Luhmann et al. (2017)). The structural properties of the entire turbine have been modeled starting

https://doi.org/10.5194/wes-2020-22
Preprint. Discussion started: 19 February 2020

eawe european academy of wind energy
Open Access WIND ENERGY SCIENCE DISCUSSIONS

from the provided HAWC2 aeroelastic data. A multi-body system consists of rigid or flexible bodies interconnected by force and joint elements that impose the kinematic and dynamic constraints. Each body, represented by one or more markers, may then have three translational and rotational displacements as result of deformations and motion. The body motion is described by a set of Differential-Algebraic Equations (DAEs), a combination of differential motion equations and algebraic constraints. The blades are modeled as nonlinear SIMBEAM body types discretized into 22 Timoschenko elements in radial direction, taking into consideration also gravitational and centrifugal forces. Structural damping is applied using the Rayleigh damping model with $\alpha = 0.025$ and $\beta = 0.014$. The tower, due to its small expected deflections, has been modeled as a linear SIMBEAM discretized into 25 Euler-Bernoulli elements, the hub has been modeled with 2 linear Euler-Bernoulli elements and the nacelle is modeled with one only rigid node, i.e. it can move but not deform, see fig. 2. Loads provided from the CFD are damped for the first 200 timesteps (equivalent to 200 Azimuth degrees) in order to avoid strong and fast deformations that can lead to instability in the calculation.

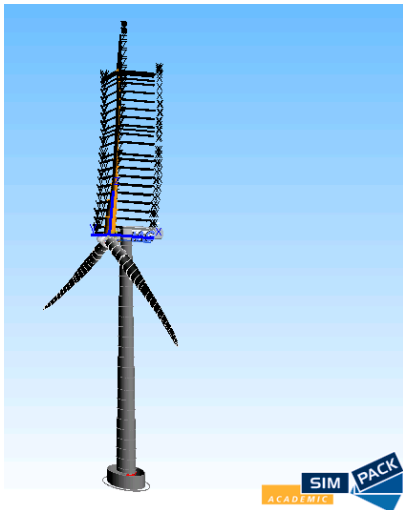

(a)

Figure 2. Details of the structural MBD model

2.4 FSI setup and computed cases

In order to allow the communication between FLOWer and SIMPACK, moving, undeformed and reference system markers need to be defined as prescribed in (Klein et al. (2018)). In the present study no controller is taken into account, that is why each simulation is conducted with a fixed rotational speed and pitch. The used coupling algorithm is explicit, i.e. deformations and loads are exchanged only once per physical timestep. In particular, the loads at the end of the flow calculation timestep are used to calculate deformations that are applied to the subsequent step, see fig. 3. The chosen timestep in this case is 1 azimuthal degree. An already converged rigid simulation of the turbine that ran already for at least 24 revolutions is used as restart for the

https://doi.org/10.5194/wes-2020-22
Preprint. Discussion started: 19 February 2020

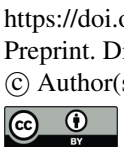

eawe european academy of wind energy
Open Access WIND ENERGY SCIENCE DISCUSSIONS

coupled simulation in order to speed up the calculation and save computational time.

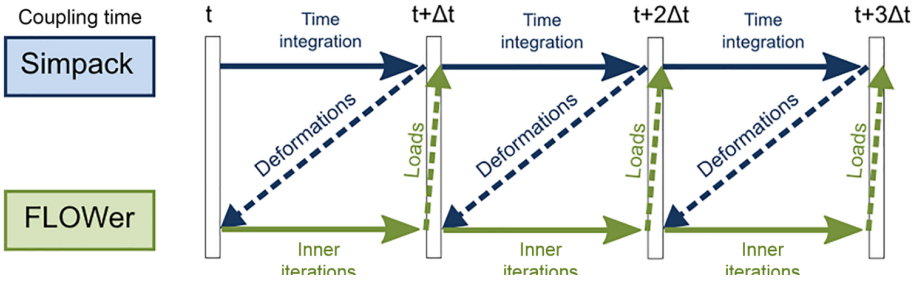

(a)

Figure 3. Explicit coupling strategy

For the BMU case it was sufficient to run the coupled simulations only 6 revolutions further to achieve convergence and periodicity of the results. For the FMU, RMU and FMT at least 10 revolutions have been run, although periodicity cannot be reached in the FMT case because the simulation time is much shorter than the length of the used Mann box. The elapsed time for the coupled simulations (starting from a rigid converged solution) varies from a minimum of 15 hours with 1632 processors for the BMU to a maximum of 48 hours with 4320 processors for the FMT case. All the simulations are run on the SuperMUC-NG cluster at the Leibniz-Rechenzentrum in Munich.

In table 1 can be seen all the CFD-MBD computed cases and differences.

Case Name	Inflow Conditions	CFD Structures	Flexible Structures
BMU	uniform	one blade and 1/3 hub	blade
RMU	uniform	rotor, nacelle, tower	rotor
FMU	uniform	rotor, nacelle, tower	rotor, nacelle, tower
FMT	sheared turbulent inflow	rotor, nacelle, tower	rotor, nacelle, tower

Table 1. Computed cases with inflow condition, CFD modeled structures and flexibility

2.5 Damage Equivalent Loading (DEL)

The DEL is a constant load that leads, when applied for a prescribed number of cycles, to the same damage as that caused by a time varying load over the same period. With this method, two or more signals can be easily compared in order to get insight into the fatigue loadings that blades are facing during normal operation. The approach is based on the S-N curves (stress vs number of cycles) of the material on a log-log scale, so that the material behavior is defined by the slope of a line. Additionally a rainflow algorithm is applied to recognize in a load signal the relative fatigue cycles by filtering peeks and valleys. This algorithm allows to estimate the amount of loads change depending on the amplitude of the cycle. In this way closed stress

https://doi.org/10.5194/wes-2020-22
Preprint. Discussion started: 19 February 2020

eawe european academy of wind energy
Open Access WIND ENERGY SCIENCE DISCUSSIONS

hysteresis cycles can be identified defining not only their amplitude but also how often they appear. The consequent damage is in fact dependent on the combination of the last two factors. The used formulation in this paper is the one from Heindrinks et al. (Hendrinks et al. (1995)) in which the different load signals are compared based on a quantitative basis and taking into account not only the range but also the mean of the load cycles. According to this method, the final expression of the DEL resulting from a prescribed signal is:

$$DEL = S_{r,eq} = \left(\sum_{i=1}^{n} \frac{\left(S_{r,i} * \frac{S_u - S_{m,eq}}{S_u - S_{m,i}} \right)^m}{Neq} \right)^{\frac{1}{m}} \tag{1}$$

In which n is the total number of cycles detected by the rainflow counting, $S_{r,i}$ is the amplitude of the $i-th$ cycle, S_u is the ultimate load, $S_{m,i}$ is the mean value of the i cycle, Neq is the number of cycles corresponding to DEL, $S_{m,eq}$ is the equivalent mean value of the cycle with amplitude DEL and, finally, m is the slope of the S-N curve considering a symmetric Goodman diagram with straight life lines.

$S_{r,i}$ and $S_{m,i}$ are a direct output of the rainflow counting, meaning that they are an individual and inevitable characteristic of the spectrum itself. Differently, Neq, S_u, $S_{m,eq}$ and m need to be chosen in advance. S_u and m are material dependent, where a log-log S-N curve is considered in order to have a straight line, respectively a constant m, while S_u can be calculated in first approximation as 5 times the maximum load in the provided spectrum. Neq and $S_{m,eq}$ are only user dependent. It is then clear that the absolute value computed by the DEL strongly depends on the choice of the constants, but as long as the same constants are considered, the DEL values are consistent within each other and, therefore, comparable.

3 Results

3.1 Aeroelastic effects

In this first section, the effects of aeroelasticity on the reference wind turbine are analyzed. The considered DANAERO experiment was performed at a low inflow velocity ($6.1m/s$), that is why it is expected to have small deformations, and therefore especially a low tower effect. The used structural model is always the same, switching opportunely the flexible components to rigid as prescribed in table 1. This means that the calculation of gravitational and centrifugal forces, that is made directly in SIMPACK, is always taking the tilt angle into account, even in the BMU case. Firstly, as validation of the results, the sectional normal and tangential loads according to the chord length for 3 different radial positions in comparison to experiments are shown in fig. 4, where a good agreement can be noticed.

https://doi.org/10.5194/wes-2020-22
Preprint. Discussion started: 19 February 2020

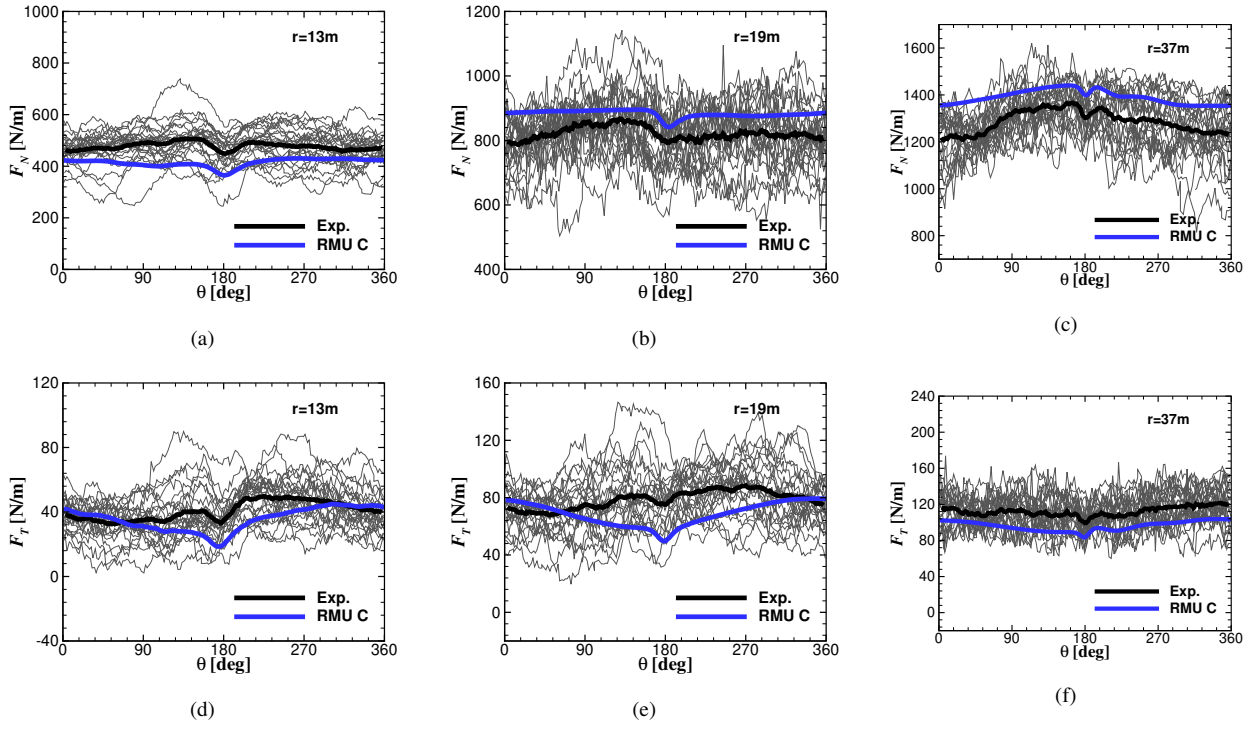

Figure 4. Comparison of experimental normal and tangential loads for three sections over the blade. In this case only the blades are considered flexible.

3.1.1 BMU vs RMU

The first considerations are made comparing cases BMU and RMU, that differ from each other by the presence of a rigid tower and a CFD model without tilt. Deformations in flap-wise, edge-wise and torsion direction of the tip of the blade can be seen in fig. 5. It can be noticed that, due to the inertia of the blade, the tip deformation starts its downturn by 180° but shows its minimum with a delay of around 20°.

A clear sinusoidal trend can be seen in both cases, that leads to an oscillation of the tip deflection from 2.27% to 2.47% of the blade radius for the BMU case, and from 2.53% to 2.25% for the RMU case. This oscillation shows in RMU to be stronger than the blade-tower passage, therefore after the minimum due to the blade-tower interaction, there is a recovery that immediately collapses in order to follow the sinusoidal trend. This difference in the maximum deflection between BMU and RMU is 2.4% and is due to a higher oscillation of the affecting loads in RMU already in the rigid case, as can be seen in fig. 6 where the global thrust (F_x) and torque (M_x) in the rigid and coupled case on the blade are plotted.

The sinusoidal behavior in the tip deflection is due to the presence of the tilt (5°), by which the gravitational and centrifugal forces produce an oscillating deformation component in flap-wise direction. Diversely, the aerodynamic contribution remains almost constant in time, with an oscillation smaller than 1%. As previously mentioned, the CFD model in BMU presents no

https://doi.org/10.5194/wes-2020-22
Preprint. Discussion started: 19 February 2020

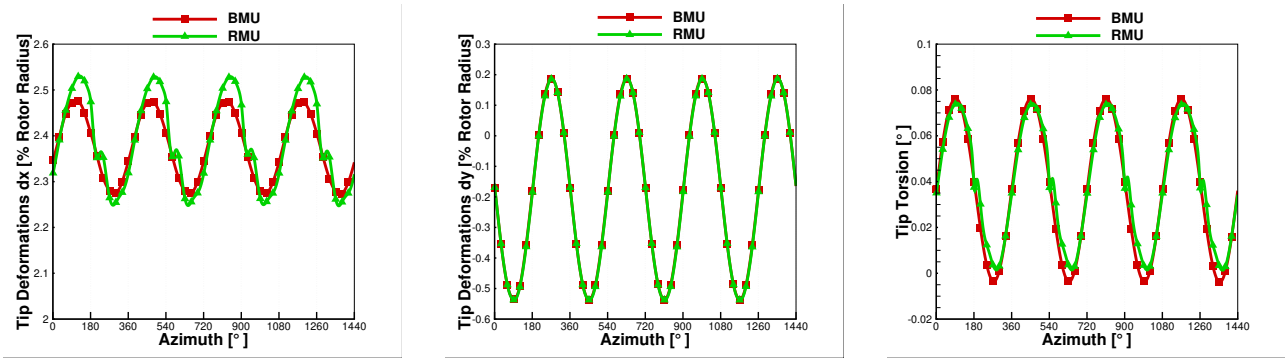

(a) Flap-wise (b) Edge-wise (c) Torsion

Figure 5. Tip deformations in comparison BMU vs RMU

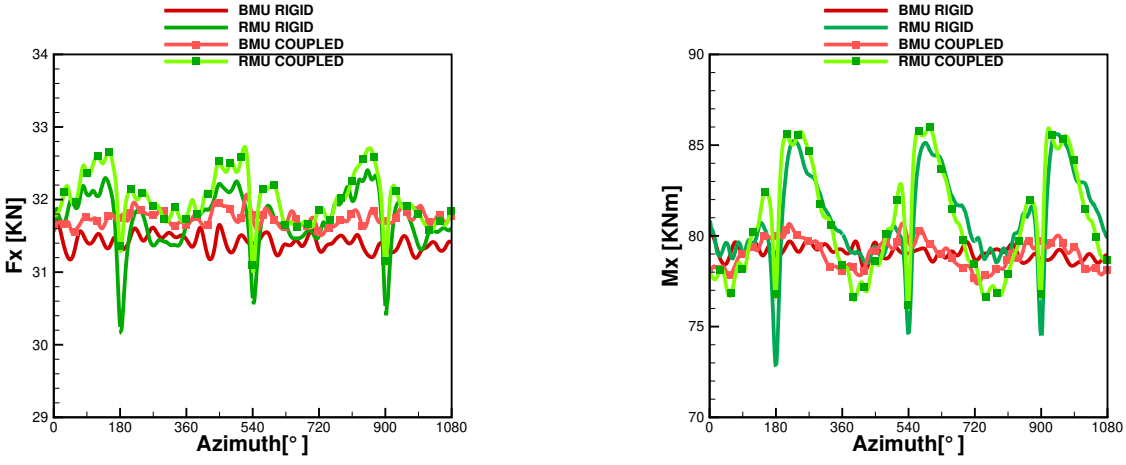

(a) Thrust (b) Torque

Figure 6. Thrust and torque in comparison BMU vs RMU, both rigid and coupled

tilt, but the structural model does, that it why the resulting centrifugal and gravitational forces are accordingly affected. This leads to the oscillation also in the response of BMU.

The tip deformations in edge-wise direction differently, being only dependent on the gravitational forces, show almost no difference between BMU and RMU. The same conclusion can be drawn for the torsion, which minimum value is slightly lower in RMU, but at the end not of interest due to its really low maximum value of 0.075°.

Focusing on the global thrust and torque in the BMU case between rigid and coupled, it can be seen that M_x in 6 has an oscillatory trend, directly related to the sinusoidal oscillation of the blade. The global thrust is slightly shifted to higher values in case of coupling, by which the mean value increases of 1%. This is due to the deformation of a pre-bended blade, resulting in an increase of the effective rotor surface. Even if the torque oscillates more in flexible case than in rigid state, the average

https://doi.org/10.5194/wes-2020-22
Preprint. Discussion started: 19 February 2020

eawe european academy of wind energy
Open Access WIND ENERGY SCIENCE DISCUSSIONS

difference is lower than 0.1% and therefore negligible. The RMU case shows a larger oscillation due to the tower passage and as in the BMU case, the structural coupling leads to a shift of both thrust and torque curves to higher values. In particular, directly before the tower passage, the flexible blade reaches higher values of thrust (in average 1 to 2% more) with a consequent higher thrust in front of the tower (in average 2 to 3% more). The same effect, although less evident, can be seen for the torque. Averaging over three revolutions, the maximum difference in the produced power is up 2.3% and can be seen between the rigid BMU and the flexible RMU. Lastly, the difference in the sectional loads is analyzed in fig. 7, averaged over the last revolution. These are the sectional forces normal and tangential to the rotor plane.

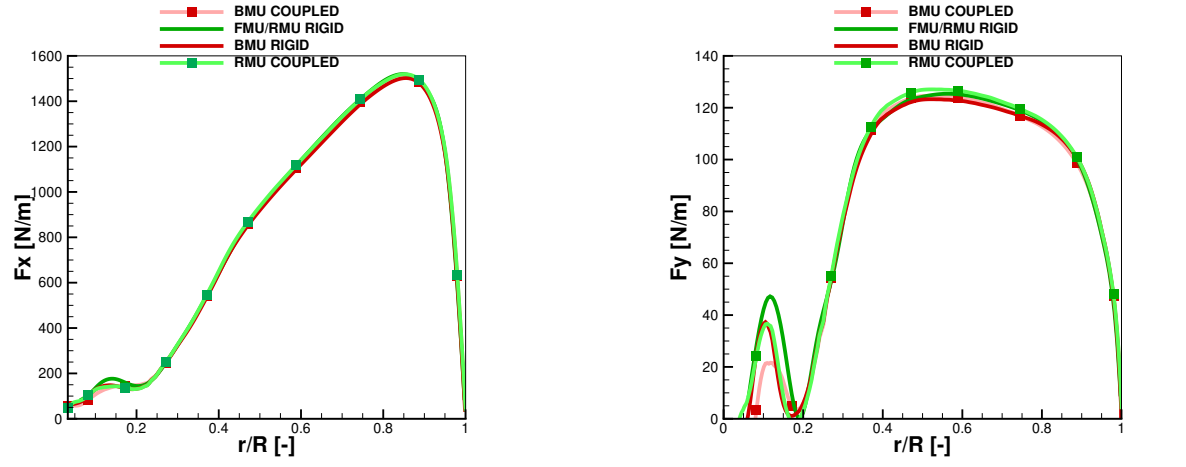

(a) Fx

(b) Fy

Figure 7. Normal and tangential sectional loads in comparison BMU vs RMU, both rigid and coupled

The normal forces between coupled and rigid show almost no difference. In the tangential loads, the one generating the power at the shaft, it can be seen that between 40% and 60% of the blade radius a small increase can be observed (around 1%), due to a local slightly higher angle of attack (around 0.8 % more), connected with the positive value of torsion showed before, and due to the increase of the effective rotor area.

3.1.2 RMU vs FMU

As mentioned in section 2.4, the difference between RMU and FMU lays in the flexibility of tower and nacelle. The flap-wise, edge-wise and torsion deformations in comparison between RMU and FMU can be seen in fig. 8. Due to the low inflow velocity, the tower deflection contributes to the total blade out-of-plane deflection for only 0.1% of the blade radius.

For the edge-wise deflection, the average value increases from 0.43% of the blade length for RMU to 0.65% for FMU due to the additional contribution of the tower top deformation. For the same reason aforementioned, the torsion deflection has in average the same value, but shows a higher amplitude of the oscillation that increases in the FMU case up to 17% more. The global thrust (F_x) and torque (M_x) for the RMU and FMU rigid and coupled can be seen in fig. 9. 1% deviation can be seen by

https://doi.org/10.5194/wes-2020-22
Preprint. Discussion started: 19 February 2020

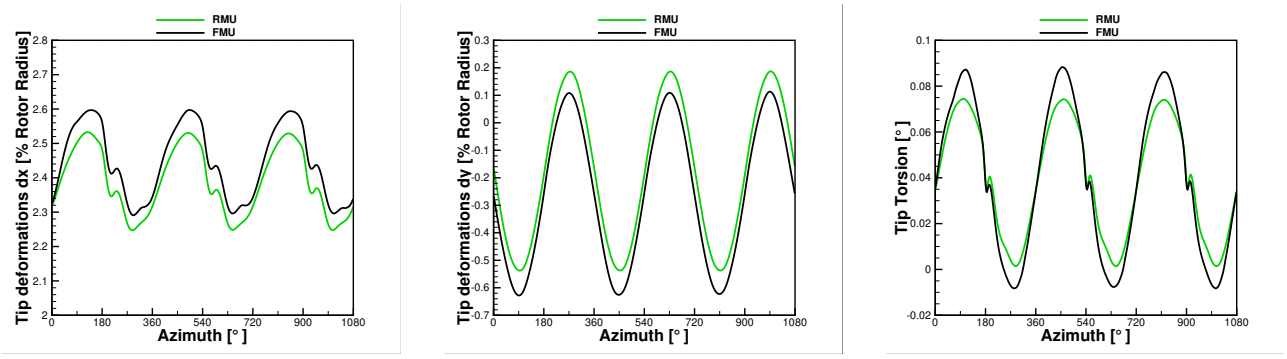

(a) Flap-wise (b) Edge-wise (c) Torsion

Figure 8. Tip deformations in comparison RMU vs FMU

addition of flexibility, although almost no difference is shown between RMU and FMU coupled due to the small deflections of the tower top.

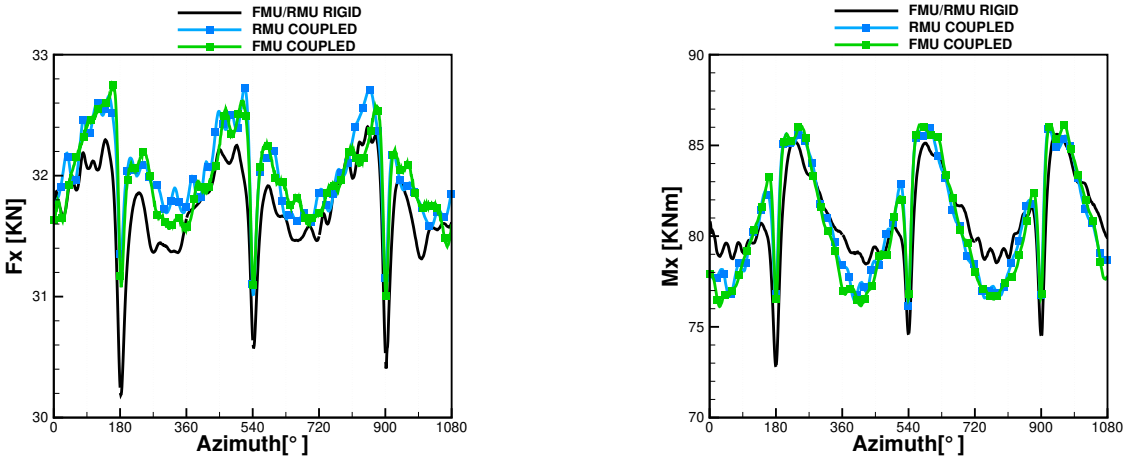

(a) Thrust (b) Torque

Figure 9. Thrust and torque in comparison RMU vs FMU, both rigid and coupled

Focusing only on the difference in FMU between rigid and coupled, it can be seen that the decay due to the tower passage is decreased up to 6%. This has a direct effect on the maximum value reached directly after the recovery, that is also always higher than in the rigid case. It can also be observed that within one revolution the amplitude of the oscillation is higher in the coupled simulation. Averaging the results over the revolutions, it results that the coupled case produces 3.5% more power than the rigid case. In order to understand this behavior, the sectional loads of the in FMU rigid and coupled are compared taking into account the average over the last revolution, see fig. 10. The area of interest is from 20% of the blade radius, because near the hub the difference between the two curves is mostly due to the strong unsteadiness affecting the hub region, where

https://doi.org/10.5194/wes-2020-22
Preprint. Discussion started: 19 February 2020

eawe european academy of wind energy
Open Access WIND ENERGY SCIENCE DISCUSSIONS

separation is occurring. As it can be seen the loads in normal direction F_x are not affected at all by the coupling. Differently the tangential loads F_y, that are also the ones generating the torque M_x and therefore the power, show some difference in the range between 40% and 70% of the blade radius (around 2 % more). This effect was also discussed by Sayed et al. (2016), who explained it with a slight increase of the angle of attack in this region. Differently from 70% of the blade length, where due to a decrease of the angle of attack, the loads for the couple simulations were lower than in the rigid case resulting in a decrease of the total power. In the present study, differently, there is almost no difference in the outer region of the blade, that is why the power increases.

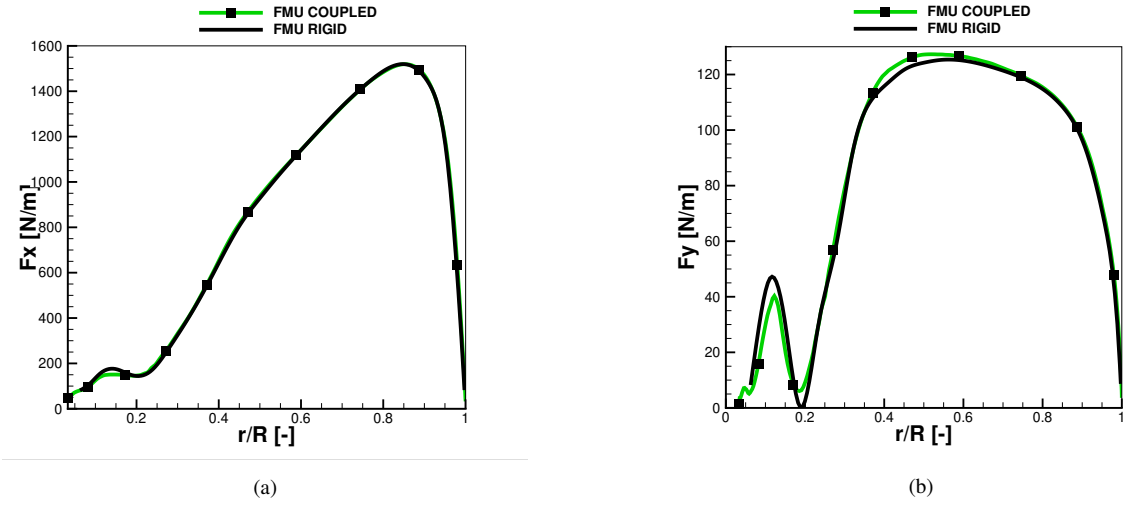

(a) (b)

Figure 10. Sectional loads comparison in FMU both rigid and coupled

3.1.3 FMU vs FMT

Figure 11 shows iso-surfaces of the λ_2-criterion for both inflow cases. The interaction of the near wake vortices and the Karman vortex street of the tower can be seen. The tower in fact faces not only the turbulence of the flow, but also the combination of the wake generated by the blades with it, resulting in a strongly turbulent flow and oscillations in the computed loads.

The comparison in the tip deformations in flap and edge direction and the torsion can be seen in fig. 12. As it can be seen, the FMU case reaches already after 2 revolutions a periodic steady state by which the blade oscillates with an average of 2.45% of the blade length. The same convergence velocity can be seen for the edge-wise deformation and for the torsion, both of them almost negligible. All the three are oscillating according to the rotational frequency.

The flap and torsion deformations show to be mostly affected by the presence of turbulence. In particular in flap direction 5 major peaks in 10 revolutions can be observed where the maximum deformation is around 3.1% of the blade length, that is 47% higher than the maximum in the uniform case. At the same time the minimum flap-wise displacement, that is not due to the tower passage, is 30% lower than in the uniform case. In case of the torsion deformations, the turbulence is mostly affecting

https://doi.org/10.5194/wes-2020-22
Preprint. Discussion started: 19 February 2020

(a) FMU

(b) FMT

Figure 11. Visualization of the λ_2 criterion

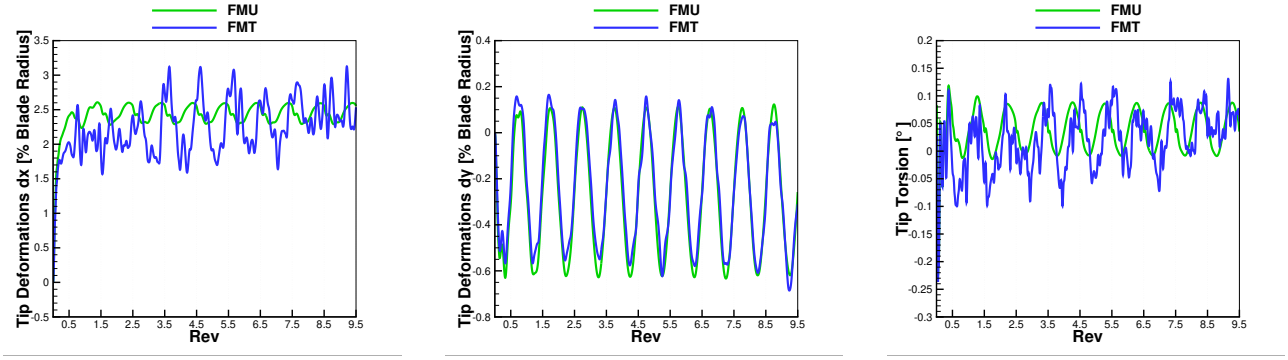

(a) Flap-wise

(b) Edge-wise

(c) Torsion

Figure 12. Tip deformations in comparison FMU vs FMT

the minima, that for FMU is -0.008°, while for FMT is -0.09°. In the defined coordinate system, a negative torsion moves the trailing edge more downwind. The edge-wise displacement, although in both cases oscillating around a mean value of 0.22%, shows revolutions in FMT always a higher for the first 8 minimum.

This can be explained looking at the tower top deformations in flap-wise direction, see fig. 13. In fact, in FMT the tower displacement is always smaller than in the FMU, and the tower deflection has an additional tilting effect on the rotor and consequently on the gravitational forces. After the eighth revolution, shows the tower top larger peaks in FMT as in FMU, leading to the opposite effect and that is why to a smaller peak in the edge-wise deformation.

https://doi.org/10.5194/wes-2020-22
Preprint. Discussion started: 19 February 2020

eawe european academy of wind energy
Open Access WIND ENERGY SCIENCE DISCUSSIONS

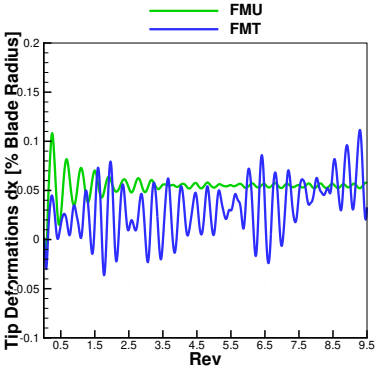

(a)

Figure 13. Tower top deformation in flap-wise direction

The spectra of the deformations is depicted in fig. 14, where the rotor frequency together with the higher harmonics are always marked by a symbol. In flap-wise direction an increase of the amplitude of the harmonics of the rotor frequency can be seen, where especially the first one shows the strongest increase. In particular it can be seen that in FMT a peak appears close to the first flap bending eigenfrequency of the blade ($f_1 = 0.938Hz$) that could lead to instabilities. Additionally it can be recognized that due to the inflow turbulence in FMT, in the broadband of the spectrum are the higher harmonics of the rotor frequency obscured. In edge-wise direction, that is mostly influenced by gravitation and not from aerodynamics, no strong increase can be seen for the rotor frequency, and the same happens for the torsion. Differently is for the broadband that always has a higher amplitude in FMT than in FMU.

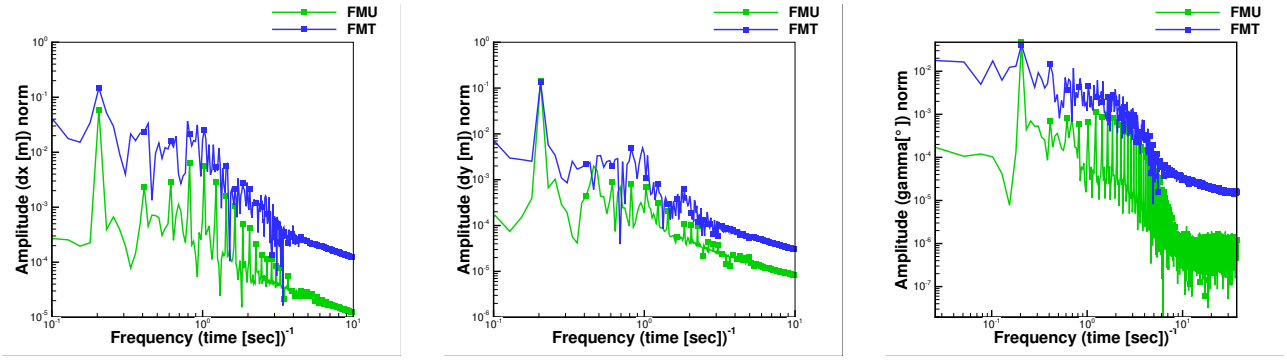

(a) Flap-wise (b) Edge-wise (c) Torsion

Figure 14. Spectra of the deformations in comparison FMU vs FMT

The effect of the tower can be again recognized in both FMU and FMT with a delay of around 20°, where a sudden drop in the tip deformations can be seen, see fig. 12. Nevertheless this drop is almost negligible in comparison to the total affecting oscillation.

https://doi.org/10.5194/wes-2020-22
Preprint. Discussion started: 19 February 2020

eawe european academy of wind energy
Open Access WIND ENERGY SCIENCE DISCUSSIONS

After analyzing the resulting deformations, some considerations on the resulting loads in the case FMT are now made (FMU has been already discussed in section 3.1.2), see fig. 15. Independently of the rigidity of the structure, the turbulence leads to a much higher amplitude in the oscillation of the loads in comparison to FMU, see 9. In fact, looking at the torque M_x, it fluctuates between 140 KNm and 10 KNm, when in FMU ranges between 86 KNm and 72 KNm. Due to this high oscillation, the blade-tower passage can be hardly recognized. Differently from the FMU case, the addition of flexibility has not marked consequences neither in thrust nor in torque. Some peaks are increased in the flexible case like for example in both thrust and torque at 250°, 315 °, 700° and 1000°. Averaging the result in time, the torque is increased by the flexibility by 2.5% (against 3.5% in the uniform case). As for the blade-tower passage, the fluctuation inducted by the turbulence is the predominant source of oscillation, that is why the flexibility represents only a secondary impact. This is valid of course only for this case, where the inflow velocity and therefore the consequent deformations are small. In fig. 16 the sectional loads average over the same revolution for both rigid and coupled are plotted. It can be seen that although the shape of F_y has changed between 30% and 70% of the blade length due to the strong oscillation brought by the turbulence, almost no difference can be seen by the inclusion of flexibility.

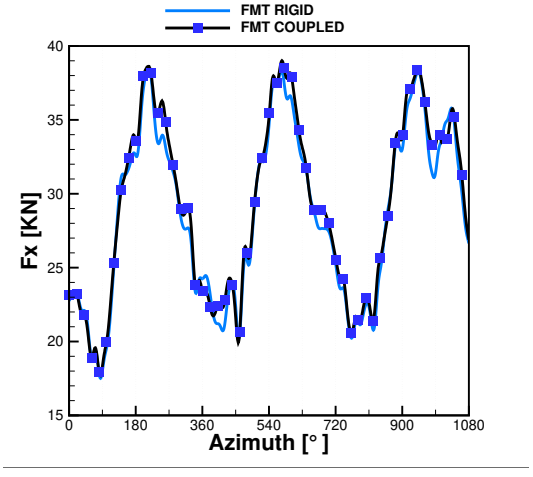

(a) Thrust

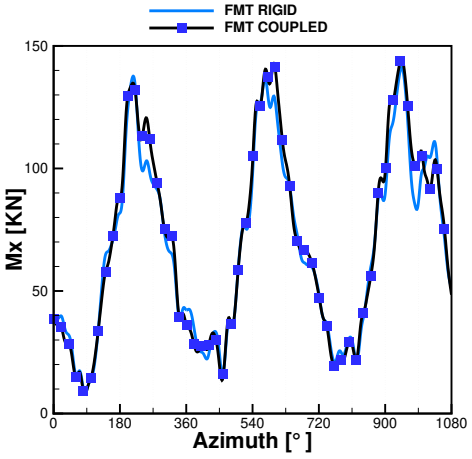

(b) Torque

Figure 15. Global loads in FMT: comparison between rigid and coupled

3.2 DEL analysis

As a further reflection of the effects of aeroelasticity in the different considered cases, comparisons in fatigue loading are now made. For this case the necessary constants described in section 2.5 have been set to $Neq = 10^5$, $S_{m,eq} = 0$ and $m = 11$, where the last one is material dependent. The first two, as described in Hendrinks et al. (1995), are not influencing the results, because when making fatigue comparison, it is not the absolute value, rather the relative value between the output from two signals, to be of interest. The input signal chosen for the analysis are the flap-wise and edge-wise blade root moment, M_y and M_x

https://doi.org/10.5194/wes-2020-22
Preprint. Discussion started: 19 February 2020

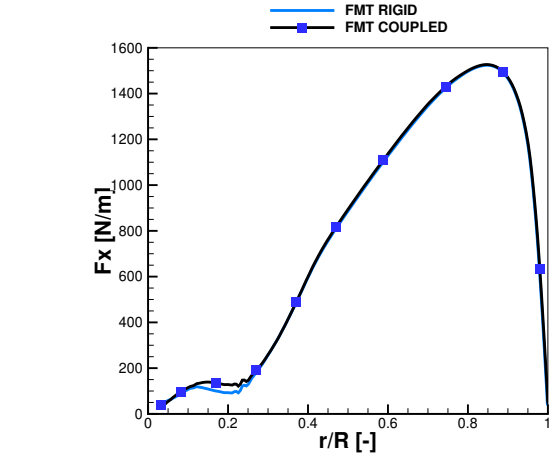

(a) Sectional normal loads

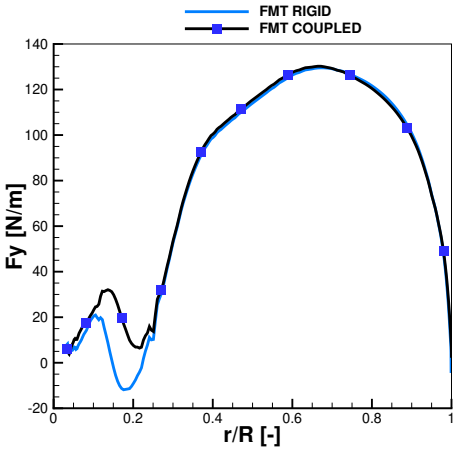

(b) Sectional tangential loads

Figure 16. Sectional loads in FMT: comparison between rigid and coupled

respectively. The first one represents in fact an unwanted action of the wind on the blade, while the second one is the one producing power.

Results are displayed in fig. 17, normalized to the lowest fatigue load calculated, i.e. BMU in rigid case.

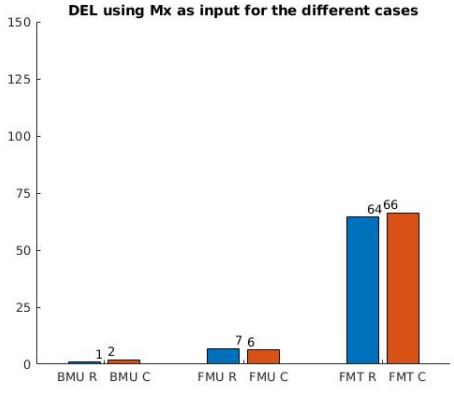

(a) DEL from Mx

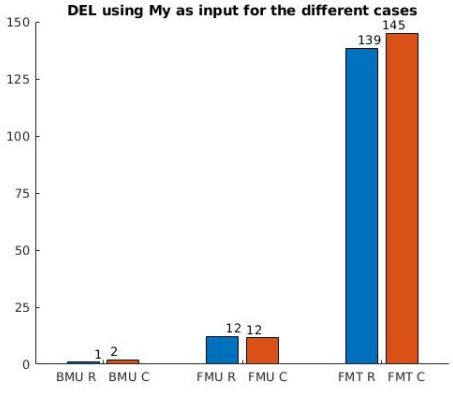

(b) DEL from My

Figure 17. DEL calculation for the different cases using in 17a M_x and in 17b M_y; R and C stays for "rigid" and "coupled"

It can be seen that switching in BMU from rigid (R) to coupled (C), almost the same increase in fatigue can be seen for both inputs, that is two times the fatigue in rigid case. In fact it can be observed in fig. 18a that the flexibility increases mainly the number of small cycles of the signal (fluctuations) and adds a few cycles with higher amplitude. In the case of FMU, already in rigid there is an increase of 7 times the fatigue in comparison to BMU, due to the tower passage and this effect is more

https://doi.org/10.5194/wes-2020-22
Preprint. Discussion started: 19 February 2020

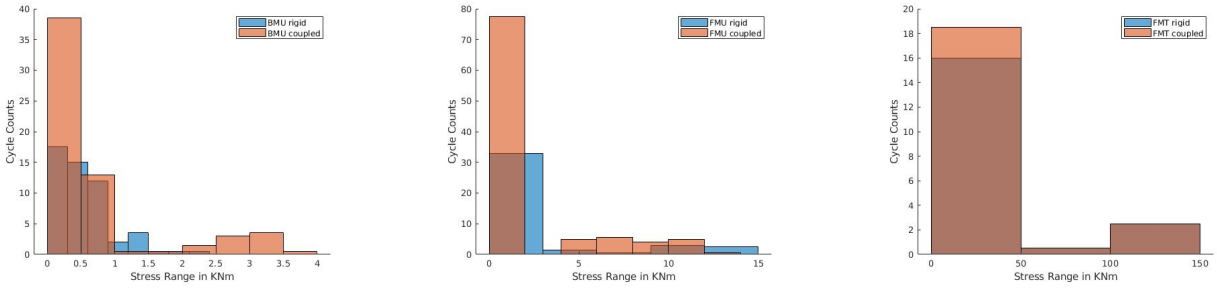

(a) BMU (b) FMU (c) FMT

Figure 18. Comparison of number of cycles counts to stress ranges using M_x as input

highlighted using as input M_y. What is interesting to observe is that the coupling in this case has almost no effect on the total damage. This is because as shown in section 3.1, the flexibility has two compensating effects on the loads: on the one side the increase of the oscillations and their mean value, and on the other side the decrease of the blade-tower passage effect. These two effects almost counter act each other leading in total to a comparable value of fatigue.

In FMT it can be seen that there is an increase in DEL from rigid to flexible because, as it can be seen from fig. 18c, the flexibility adds a few more small cycles but no big cycles, that are completely dominated by the impact of turbulence. Independently from the chosen input, the addition of turbulence increases drastically the fatigue. Much less cycles are detected by the rainflow counting, but they all have an amplitude bigger than the biggest cycles in FMU and BMU.

4 Conclusions

In the present work, different CFD models of the DANERO turbine rotor were generated and coupled to a MBD structural model of the same turbine, by means of a loose (explicit) coupling. The aeroelastic response of the reference turbine by the use of models increasing their complexity and fidelity was calculated. The effects of a turbulent inflow conditions in comparison to uniform inflow were analyzed, showing that in this case turbulence has a major effect than flexibility and blade-tower passage together. The consequent fatigue loading in the difference cases was compared and discussed, showing that for small inflow velocities, a high turbulence has the major impact on the fatigue, where the flexibility has a negligible contribution.

Author contributions. G. Guma generated part of the CFD model, the MBD model, ran the coupled simulations, and performed the post processing and analysis. G. Bangga generated part of the CFD model. T. Lutz and E. Krämer supported the research, defined and supervised the work and revised the manuscript.

Competing interests. The authors declare that they have no conflict of interest.

https://doi.org/10.5194/wes-2020-22
Preprint. Discussion started: 19 February 2020

Acknowledgements. The authors gratefully acknowledge the DANAERO Consortium for providing the geometry and structural data. They acknowledge additionally SIMPACK for providing the user licenses and the funders of the project WINSENT (Code number: 0324129), the Federal Ministery for Economic Affairs and Energy (BMWi) and the Ministery of the Environment, Climate Protection and the Energy Sector Baden-Württemberg under the funding number “L75 16012”, under which project improvements on the simulation chain were performed. Computer resources were provided by the Gauss Centre for Supercomputing/Leibniz Supercomputing Centre under grant "pr94va". Additionally a particular thank is given to the DLR and SWE-University of Stuttgart for the productive discussions that helped improving the structural model of these simulations.

https://doi.org/10.5194/wes-2020-22
Preprint. Discussion started: 19 February 2020

eawe european academy of wind energy
Open Access WIND ENERGY SCIENCE DISCUSSIONS

References

DANAERO project; http://www.dan-aero.dtu.dk/; 28.01.2020;

IEA Task 29; https://community.ieawind.org/task29/29workplan; 28.01.2020;

Bazilevs, Y., Hsu, M.C., Kiendl, J., Wüchner, R., Bletzinger, K.U.; 3d simulation of wind turbine rotors at full scale. prt ii: Fluid–structure interaction modeling with composite blades. International Journal for Numerical Methods in Fluids 65, 236–253; 2011b;

Boorsma, K., Wenz, F., Aman, M., Lindenburg, C., Kloosterman, M.; TKI WoZ VortexLoads, Final report; TNO 2019 R11388; 2019;

Dose, B., Rahimi, H., Herráez, I., Stoevesandt, B., Peinke, J.; Fluid-structure coupled computations of the nrel 5 mw wind turbine by means of cfd; Renewable energy 129, 591–605; 2018;

Hansen M.O.L. and Sørensen J.N. and Voutsinas S. and Sørensen N. and Madsen H.Aa.; State of the art in wind turbine aerodynamics and aeroelasticity; Progress in Aerospace Sciences, 42, 4, 285-330; 2006;

Heinz, J.C., Sørensen, N.N., Zahle, F.; Fluid–structure interaction computations for geometrically resolved rotor simulations using cfd; Wind Energy 19, 2205–2221; 2016;

Hendriks H.B. and Bulder B.H. Fatigue Equivalent Load Cycle Method; ECN Publicaties; 1995;

Hsu, M.C., Bazilevs, Y.; Fluid–structure interaction modeling of wind turbines: simulating the full machine; Computational Mechanics 50, 821–833; 2012;

Jameson A. and Schmidt W. and Turkel E. et al.; Numerical solutions of the Euler equations by finite volume methods using Runge-Kutta time-stepping schemes; AIAA Paper 81-1259; 1981;

Jassmann, U., Berroth, J., Matzke, D., Schelenz, R., Reiter, M., Jacobs, G., and Abel, D.; Model predictive control of a wind turbine modelled in Simpack; Journal of Physics: Conference Series, vol. 524, IOP Publishing; 2014;

Jeong, MS and Yoo, SJ and Lee, I; Aeroelastic analysis for large wind turbine rotor blades; 52nd AIAA/ASME/ASCE/AHS/ASC Structures, Structural Dynamics and Materials Conference, Structures, Structural Dynamics, and Materials and Co-located Conferences; AIAA; 9–14; 2011;

Klein, L and Gude, J and Wenz, F and Lutz, Th and Krämer E; Advanced CFD-MBS coupling to assess low-frequency emissions from wind turbines; Wind Energy Science 2018

Kowarsch, U., Keßler, M., and Krämer, E.; High order CFD-simulation of the rotor-fuselage interaction; 39th European Rotorcraft Forum; 2013;

Li, Y., Castro, A., Martin, J., Sinokrot, T., Prescott, W., Carrica, P.; Coupled computational fluid dynamics/multibody dynamics method for wind turbine aero-servo-elastic simulation including drivetrain dynamics; Renewable Energy 101, 1037–1051; 2017;

Luhmann, B., Seyedin, H., and Cheng, P.-W.; Aero-structural dynamics of a flexible hub connection for load reduction on two-bladed wind turbines; Wind Energy, 20, 521–535; 2017;

Madsen A. and Bak C. and Schmidt U. P. and Gaunaa M. and Fuglsang P. and Romblad J. and Olesen N. A. and Enevoldsen P.B. and Laursen J. V. and Jensen L. E.; "The DAN-AERO MW Experiments Final Report"; 2010;

Madsen, H.A., Riziotis, V., Zahle, F., Hansen, M., Snel, H., Grasso, F., Larsen, T., Politis, E., Rasmussen, F.; Blade element momentum modeling of inflow with shear in comparison with advanced model results; Wind Energy 15, 63–81; 2012;

Mann, J.; The spatial structure of neutral atmospheric surface-layer turbulence; Journal of fluid mechanics 273, 141–168; 1994;

Menter F. R.; Two equation eddy-viscosity turbulence models for engineering applications; AIAA J. 32(8), 1598-1605; 1994;

https://doi.org/10.5194/wes-2020-22
Preprint. Discussion started: 19 February 2020

Masarati, P., Sitaraman, J.; Coupled cfd/multibody analysis of nrel unsteady aerodynamic experiment phase vi rotor AIAA Aerospace Sciences Meeting and Exhibit, Orlando, FL.,AIAA Paper; 2011;

Raddatz J.; The block-structured RANS solver FLOWer; DLR, Institute of Aerodynamics and Flow Technology; 2009;

Riziotis, V.A. and Voutsinas, S.G. and Politis, E.S. and Chaviaropoulos, E.S. and Hansen, Anders Melchior and Madsen Aagaard, Helge and Flemming Rasmussen; "Identification of structural non-linearities due to large deflections on a 5MW wind turbine blade"; EWEC, Vindenergi; Scientific proceedings; 9–14; European Wind Energy Conference and Exhibition; 2008;

Sayed, M and Lutz, Th and Krämer, E and Shayegan, Sh and Ghantasala, A and Wüchner, R and Bletzinger, K-U; High fidelity CFD-CSD aeroelastic analysis of slender bladed horizontal-axis wind turbine; Journal of Physics: Conference Series; 753; 4; IOP Publishing; 2016;

Schepers, J.; Latest results from the EU project AVATAR: Aerodynamic modelling of 10 MW wind turbines; Journal of Physics: Conference Series, 753, 022 017; 2016;

Troldborg N. and Bak C. and Madsen A., Helge and Skrzypinski, Witold R.; "DANAERO MW: Final Report"; "DTU Wind Energy"; 2013;

Yu, D.O., Kwon, O.J.; Time-accurate aeroelastic simulations of a wind turbine in yaw and shear using a coupled CFD-CSD method Journal of Physics Conference Series 524, 012046; 2014;